

# Exponential time integration for 3D compressible atmospheric models

Greg Rainwater<sup>a,\*</sup>, Kevin C. Viner<sup>b</sup>, P. Alex Reinecke<sup>b</sup>

<sup>a</sup>American Society for Engineering Education, 7 Grace Hopper Ave., Monterey, CA 93943

<sup>b</sup>U.S. Naval Research Laboratory, 7 Grace Hopper Ave., Monterey, CA 93943

---

## Abstract

Recent advancements in evaluating matrix-exponential functions have opened the doors to the practical use of exponential time-integration methods in numerical weather prediction (NWP). The success of exponential methods in shallow water simulations has led to the question of whether they can be beneficial in a 3D atmospheric model. In this paper, we take the first step forward by evaluating the behavior of exponential time-integration methods in the Navy's compressible deep-atmosphere nonhydrostatic global model (NEPTUNE-Navy Environmental Prediction system Utilizing a Nonhydrostatic Engine). Simulations are conducted on a set of idealized test cases designed to assess key features of a nonhydrostatic model and demonstrate that exponential integrators capture the desired large and small-scale traits, yielding results comparable to those found in the literature. We propose a new upper boundary absorbing layer independent of reference state and shown to be effective in both idealized and real-data simulations. A real-data forecast using an exponential method with full physics is presented, providing a positive outlook for using exponential integrators for NWP.

*Keywords:* exponential integrators, numerical weather prediction, compressible, nonhydrostatic, atmospheric model, absorbing layer

---

## 1. Introduction

With the rapid and continuous evolution of atmospheric models, the development of efficient time integrators is a difficult and recurring problem. The presence of fast acoustic and gravity waves rendered the use of explicit methods inadequate due to a severely restricted time step [43]. While an implicit scheme alleviates the allowable time step size restriction, these methods are computationally intensive and deemed infeasible without a suitable preconditioner. Techniques such as filtering approximations that eliminate the acoustic waves have been used to avoid the efficiency restrictions, but are not applied in this paper. Even though such approximation was used in [36, 24], it was their introduction of the semi-implicit methods that opened the doors to efficient time integration for numerical weather prediction (NWP) models. By partitioning the dynamics such that the fast/slow waves can be handled implicitly/explicitly greatly improved the efficiency by reducing the stability constraints of the explicit methods and the complexity of the equations to be solved implicitly. [22] proposed a similar technique known as split-explicit that does not rely on any manipulations of the equation set. The split-explicit methods uses a "large" time step for slow dynamics and "small" substeps to integrate the fast dynamics. The relative simplicity and computational efficiency of the split-explicit methods made them an attractive and widely adopted time integrator for NWP [40, 46, 20].

Interest in implicit-explicit (IMEX) methods for NWP followed with the development of Runge-Kutta type IMEX methods [1, 13, 43]. [43] found that combining an explicit Runge-Kutta and linearly implicit Rosenbrock scheme provided time steps that were only restricted by the horizontal Courant-Friedrichs-Lewy (CFL) number. [9] thoroughly investigated the performance of twenty-one additive Runge-Kutta IMEX schemes for four different splitting strategies (or partitioning of the dynamics). The results in [9] indicate that Runge-Kutta IMEX schemes can offer a suitable option for global non-hydrostatic atmosphere simulations.

---

\*Corresponding author

Email addresses: grainwater@outlook.com (Greg Rainwater), kevin.viner@nrlmry.navy.mil (Kevin C. Viner), alex.reinecke@nrlmry.navy.mil (P. Alex Reinecke)

The aim of this article is to demonstrate the use of exponential integrators as an alternative time integration strategy for simulating nonhydrostatic compressible atmospheric dynamics. Similarly to implicit methods, exponential integrators possess good stability properties, but require evaluation of exponential-like, rather than rational, matrix functions. Using a Krylov-projection-based method to evaluate an exponential-like function can save a significant amount of computational time compared to the rational function evaluation needed for an implicit integrator. Exponential methods have the additional advantage of being very accurate for nonlinear systems and exact for linear systems. The computational benefits of exponential integrators can be seen across a wide range of disciplines from computer graphics [29] to magnetohydrodynamics [5]. The use of exponential methods in NWP so far is limited, but positive results were reported for simulations of the shallow water equations on the sphere in [2, 11, 27].

The paper is organized as follows. In Section 2 we provide an overview of exponential integration and the integrators we will be using for our simulations. Section 3 details our numerical experiments, where we evaluate the accuracy of the integrators and demonstrate their capabilities in simulating idealized test cases and real-data forecasts in the Navy's compressible deep-atmosphere nonhydrostatic model, NEPTUNE (Navy Environmental Prediction sysTem Utilizing a Nonhydrostatic Engine).

## 2. Exponential Integrators

The construction of exponential integrators typically begins with reformulating

$$u'(t) = f(u(t)), \quad u(t_0) = u_0, \quad u(t) \in \mathbb{R}^n \quad (1)$$

as an integral equation which involves an exponential of either the full Jacobian  $f'(u) \in \mathbb{R}^{n \times n}$  or a portion of it if a meaningful partitioning of  $f(u)$  exists (e.g. if  $f(u) = Lu + N(u)$  where  $L$  and  $N$  represent the linear and nonlinear part of  $f(u)$  respectively). As an example, consider linearizing  $f(u(t))$  around  $u_0$  using the first-order Taylor expansion such that (1) can be expressed as

$$u'(t) = f(u_0) + f'(u_0)(u(t) - u_0) + r(u(t)), \quad u(t_0) = u_0, \quad u(t) \in \mathbb{R}^n, \quad (2)$$

where  $r(u(t)) = f(u(t)) - f(u_0) - f'(u_0)(u(t) - u_0)$ . Applying the variation of constants formula to (2) yields the integral form of the solution at time  $t_0 + h$ :

$$u(t_0 + h) = u_0 + \left( \frac{e^{hf'(u_0)} - I}{hf'(u_0)} \right) hf(u_0) + \int_{t_0}^{t_0+h} e^{f'(u_0)(t_0+h-\tau)} r(u(\tau)) d\tau. \quad (3)$$

Exponential methods are derived by applying various approximations to the integral term in (3). The simplest approximation  $r(u(t)) \approx r(u_0) = 0$  produces the second-order exponential Euler (*EXP2*) method

$$u_{n+1} = u_n + \left( \frac{e^{hf'(u_n)} - I}{hf'(u_n)} \right) hf(u_n), \quad (4)$$

where  $u_n \approx u(t_n)$ . Higher-order methods are achieved by using different quadrature. However, it can be seen from (4) that the numerical solution of an exponential integrator involves the computation of an exponential-like function of a matrix. This task was deemed computationally infeasible for large scale applications until Krylov projection-based methods were used to compute the exponential of a matrix and exponentially propagate the solution of a Hamiltonian problem from chemical physics [30], and the Schrödinger equation [32]. The extension to approximating a product of an arbitrary function of a matrix and a vector (by Van der Vorst [4]) sparked interest in exponential integration with the development of many exponential propagation-based integrators [3, 6, 7, 8, 10, 15, 16, 18, 23, 28, 33, 34, 41]. The Exponential Propagation Iterative methods of Runge-Kutta type (EPIRK) [41, 42] framework has been developed to allow derivation of efficient integrators particularly for large scale stiff equations that arise from large ODE systems or spatial discretization of PDEs. The general formulation of an  $s$ -stage EPIRK method for the initial value problem (1)

is given by

$$U_{ni} = u_n + a_{i1}\psi_{i1}(g_{i1}h_n A_{i1})h_n f(u_n) + \sum_{j=2}^{i-1} a_{ij}\psi_{ij}(g_{ij}h_n A_{ij})h_n \Delta^{(j-1)}r(u_n), \quad i = 2, \dots, s \quad (5)$$

$$u_{n+1} = u_n + b_1\psi_{(s+1)1}(g_{(s+1)1}h_n A_{(s+1)1})h_n f(u_n) + \sum_{j=2}^s b_j\psi_{(s+1)j}(g_{(s+1)j}h_n A_{(s+1)j})h_n \Delta^{(j-1)}r(u_n), \quad (6)$$

where  $u_n$  is an approximation to the solution at some time  $t_n$ ,  $h_n = t_{n+1} - t_n$  is the time step and  $\Delta^{(s)}$  denotes the forward difference operator constructed on stage-values  $u_n, U_{n2}, \dots, U_{ns}$  and is given by

$$\Delta^k r(u_n) \equiv \sum_{m=0}^{k-1} (-1)^m \binom{k}{m} r(U_{n(k-m+1)}). \quad (7)$$

Different choices for functions  $r(u)$ ,  $\psi_{ij}$  and matrices  $A_{ij}$  result in different classes of EPIRK methods [35]. According to our previous example using  $r(u)$  as the first order Taylor expansion of  $f(u)$ , we take all matrices  $A_{ij} = f'(u_n)$  to be the Jacobian evaluated at  $u_n$  and functions  $\psi_{ij}(z) = \sum_{k=1}^p p_{ijk}\varphi_k(z)$  are linear combinations of the exponential-like functions

$$\varphi_0(z) = e^z, \quad \varphi_k(z) = \int_0^1 e^{(1-\theta)z} \frac{\theta^{k-1}}{(k-1)!} d\theta, \quad k \geq 1. \quad (8)$$

These choices result in a class of general (unpartitioned) EPIRK methods which are appropriate for cases where no meaningful partitioning exists for the operator  $f(u)$  and the problem's stiffness comes from the full Jacobian matrix  $f'(u_n)$ . Specific schemes can be constructed by deriving order conditions and solving to determine coefficients  $a_{ij}$ ,  $b_j$ , and  $p_{ijk}$  ([42, 41, 34]). A closely-related class to the (unpartitioned) EPIRK schemes are the Exponential Rosenbrock (EXPRB) methods [16, 26]. In [34] it was shown that any EXPRB method can be written in EPIRK form. By specifying the coefficients  $a_{i1} = g_{i1}$  and functions  $\psi_{ij}(z) = \varphi_1(z)$  in (5), it is also possible to express the EPIRK scheme in EXPRB form.

The most efficient general exponential schemes result from coupling construction of particular integrators with the choice of an algorithm to approximate the matrix-function-vector products. In general, when no useful information on the structure or the spectrum of the matrix is available or a matrix-free implementation is necessary then Krylov projection based algorithms are the methods of choice. A particularly efficient adaptive Krylov algorithm, *phipm*, has been developed in [31]. This method allows cost efficient computation of

- (I) linear combinations of type  $\varphi_0(\tau A)b_0 + \varphi_1(\tau A)b_1 + \dots + \varphi_K(\tau A)b_K$  for a matrix  $A$ , vectors  $b_i$ ,  $i = 0, \dots, K$ , and fixed  $\tau$ ;
- (II) several terms of type  $\varphi_k(\tau A)b_k$  involving a single function  $\varphi_k$  and a vector  $b_k$  for different values of  $\tau$

Based on the ideas of *phipm*, [12] introduced a new adaptive Krylov algorithm, *KIOPS*, that significantly reduces the computational cost of computing (I) and (II).

The flexibility of the EPIRK & EXPRB framework allows construction of exponential integrators that take advantage of the efficiency of the adaptive Krylov methods (*phipm* and *KIOPS*) and reduce both the number and the cost of the matrix function vector products evaluations [12, 34, 25]. The exponential integrators we consider for our numerical experiments are a selection of such methods:

- *Exponential Euler (EXP2)* - stiffly accurate second-order integrator

$$u_{n+1} = u_n + \varphi_1(h_n J_n)h_n f(u_n)$$

- *EPIRK4s3* [35, 29] - stiffly accurate fourth-order integrator

$$\begin{aligned}
U_{n2} &= u_n + \frac{1}{8}\varphi_1\left(\frac{1}{8}h_n J_n\right)h_n f(u_n) \\
U_{n3} &= u_n + \frac{1}{9}\varphi_1\left(\frac{1}{9}h_n J_n\right)h_n f(u_n) \\
u_{n+1} &= u_n + \varphi_1(h_n J_n)h_n f(u_n) + (1892\varphi_3(h_n J_n) - 42336\varphi_4(h_n J_n))h_n \Delta r(u_n) \\
&\quad + (1458\varphi_3(h_n J_n) - 34992\varphi_4(h_n J_n))h_n \Delta^2 r(u_n)
\end{aligned}$$

- *EXPRB42* [25] - stiffly accurate fourth-order integrator

$$\begin{aligned}
U_{n2} &= u_n + \frac{3}{4}\varphi_1\left(\frac{3}{4}h_n J_n\right)h_n f(u_n) \\
u_{n+1} &= u_n + \varphi_1(h_n J_n)h_n f(u_n) + \frac{32}{9}\varphi_3(h_n J_n)h_n r(U_{n2})
\end{aligned}$$

The exponential Euler scheme requires only one evaluation of a matrix function vector product each time step, namely,  $\varphi_1(h_n J_n)h_n f(u_n)$ . Any higher-order scheme will require a minimum of two separate evaluations or calls to the adaptive Krylov algorithm. *EPIRK4s3* and *EXPRB42* are examples of fourth-order methods that require only two Krylov projections per time step. For *EPIRK4s3*, the terms  $\varphi_1(\frac{1}{8}h_n J_n)h_n f(u_n)$  and  $\varphi_1(\frac{1}{9}h_n J_n)h_n f(u_n)$  are of type (II) and can be computed using a single call to the *KIOPS* algorithm. The second call is necessary for the evaluation of the terms (which are of type (I)) that appear in the final stage calculation. The situation is similar for *EXPRB42*, except that the first projection only computes one term ( $\varphi_1(\frac{3}{4}h_n J_n)h_n f(u_n)$ ). While efficient fifth-order methods have been constructed (see [34, 26]), they require three or more Krylov projections per time step; since the major computational cost of exponential integrators is the evaluation of these matrix function vector products, it is unreasonable to consider these methods here.

### 3. Numerical Experiments

The purpose of our numerical experiments is to evaluate the behavior of exponential methods in a nonhydrostatic compressible global model. All of the experiments presented below were conducted in the 3D spectral-element based atmospheric model, NEPTUNE, which is a compressible deep-atmosphere nonhydrostatic global model based on the equation set Set2NC in [14]. Starting with a fundamental set of idealized test cases, we assess the accuracy and the ability to resolve both the fast and slow processes. We can confirm exponential methods produce comparable results using well-documented simulations in the literature. We conclude by showing reasonable real-data forecasts can be obtained using exponential integrators.

#### 3.1. Order verification and comparative performance

To evaluate the accuracy of the time integrators, we apply them in NEPTUNE on the gravity wave test case defined in [45]. This test case adds a potential temperature perturbation to an initially balanced atmosphere on a reduced Earth-radius sphere (1/125) that triggers the development of gravity waves. Our spatial domain was discretized using 20 elements per edge of the cubed sphere, fourth-order spectral element polynomials, and 13 vertical levels (3 vertical elements) with a model top of 10 km. This corresponds to approximately 1.5° (1.3 km) horizontal grid spacing and 0.77 km in the vertical. For each integrator, this test case is simulated for 1 hour using time steps of 1, 5, 10, and 15 seconds. A reference solution was computed using a fully explicit third-order five-stage strong-stability-preserving Runge-Kutta method (SSPRK(5,3)) [37] using a time step of 0.0001 seconds.

Figure 1(a) displays the plots of the time step versus error for the exponential methods outlined above. For convenience, lines of slope two and four are plotted (dash-dot/dashed, respectively). We can see that *EXP2* and *EPIRK4s3* achieve their full predicted order for the smaller time step sizes while *EXPRB42* shows slightly less than fourth-order. Considering all the time steps, the estimated order of convergence for the exponential methods are *EXP2* ~ 1.86, *EPIRK4s3* ~ 3.77, and *EXPRB42* ~ 3.65.

The comparative performance of the exponential integrators is shown in Figure 1(b). Since the exponential Euler method requires fewer Krylov projections per time step, it was expected to be the most efficient for any given step size. Without any regard for the accuracy, the most efficient time step for each integrator is  $h = 15$  seconds. Comparing the execution times for this step size, *EXP2* is found to be 25% / 38% faster than *EPIRK4s3*/*EXPRB42*, respectively. These

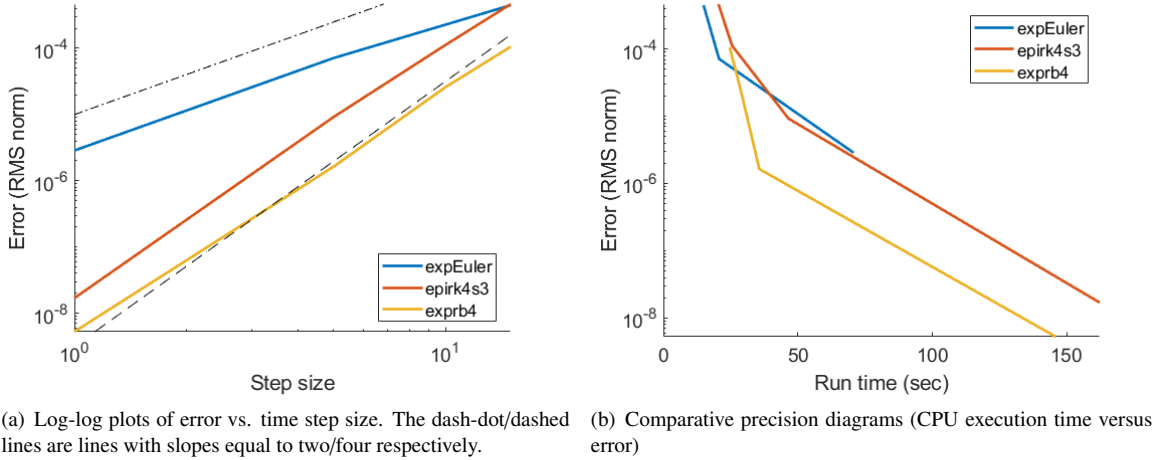


Figure 1: Order and precision diagrams for the gravity wave test case from [45]

values increase to 65% / 50% if we consider the execution times of *EPIRK4s3* and *EXPRB4* at their intersections with the graph of *EXP2* (i.e., the points at which the fourth-order methods can be of benefit) and compare them to the execution time of *EXP2* using a time step of  $h = 15$  seconds.

On the other hand, for a prescribed accuracy, the higher-order methods can offer significant computational savings. For example, if we consider a error tolerance of  $5 \times 10^{-6}$  in Figure 1(b), then *EXPRB4* is a factor of two faster than *EXP2*. The reason for this dramatic difference is that the lower order methods are forced to take a smaller step size which reduces the number of Krylov vectors per time step, but the computational cost becomes dominated by the large number of steps and the total number of Krylov vectors needed for the entire integration. The accuracy of the fourth-order exponential methods (of Runge-Kutta type) comes from taking smaller step sizes; sacrificing the competitive edge of these methods. While exponential multistep type methods [3, 41, 17] are not included here, the recent development of high-order exponential multistep schemes [10] is the next step forward in achieving high accuracy (up to order seven) at near the computational cost of *EXP2*.

### 3.2. Mountain-wave simulations

In this section we verify the ability of exponential methods to accurately capture nonhydrostatic processes by considering idealized mountain-wave test cases from [21]. These simulations are on a reduced Earth-radius sphere ( $1/166.7$ ) without rotation and designed to help evaluate the behavior of nonhydrostatic global models. [21] showed that simulations performed with the Model for Prediction Across Scales (MPAS) were in close agreement with analytical solutions of similar test case(s) in a Cartesian geometry [38]. The results in [21] will serve as baseline for our comparisons.

The mountain-wave simulations from [21] put to use an implicit Rayleigh damping of the vertical velocity [19]. The idea of [19] (with the focus on time-split integration) is to make an adjustment (on the small time steps) to the vertical velocity such that it produces a Rayleigh damping term and a (implicit) vertical diffusion term in the vertical momentum equation. Unlike the time-split integrators, exponential methods handle the fast acoustic and gravity waves via exponential-like functions and thus not able to directly apply the damping scheme from [19]. Using the same idea, we propose an effective absorbing layer via an adjustment to the vertical velocity at the end of the time step for exponential integrators. As an example, the adjustment combined with the *EXP2* method is

$$\begin{cases} \widehat{\mathbf{u}}_{n+1} = \mathbf{u}_n + h_n \varphi_1(h_n J_n) f(\mathbf{u}_n) \\ \mathbf{u}_{n+1} = \mathbf{Q} \widehat{\mathbf{u}}_{n+1} \end{cases} \quad (9)$$

where  $\mathbf{u} = (\rho, u, v, w, \theta)^T$  is the vector with density, velocities, and potential temperature as components,  $\mathbf{Q} = \text{diag}[1, 1, 1, (1 + h_n R_w)^{-1}, 1]$  and  $R_w$  is the damping profile. For our numerical experiments, we use the same damping

profile as that used in [22, 19, 21]:

$$R_w(z) = \alpha \sin^2\left(\frac{\pi}{2} \frac{z - z_h}{z_t - z_h}\right), \quad (10)$$

where  $z_t$  denotes the top of the models domain and  $z_h$  is the bottom of the absorbing layer. The adjustment to the vertical velocity in (9) filters into the other equations on the next time step calculation which produces the desired Raleigh damping term and a vertical diffusion term in the vertical momentum equation. A derivation of the exact terms is provided in Appendix A.

### 3.2.1. Quasi Two-Dimensional Mountain Ridge Case

This test case simulates the flow of an atmosphere with constant velocity over a specified mountain ridge terrain profile. The details of the terrain profile (mountain ridge) can be found in [21]. For comparison purposes, we configure our model to be as close as possible to MPAS. Thus for this test case, we specify a model top of  $z_{\text{top}} = 20 \text{ km}$ , with an upper boundary absorbing layer of depth  $z_h = 10 \text{ km}$ . We used 28 elements per face of the cubed sphere, 3rd order polynomials, and 40 vertical levels (13 elements) to obtain approximately  $1.1^\circ$  ( $720 \text{ m}$ ) horizontal grid spacing and  $500 \text{ m}$  in the vertical. The exponential Euler (*EXP2*) method was used to complete the 120 minute time integration using a time step of  $30 \text{ s}$ . Figure 2 displays the vertical velocity at 120 simulated minutes from which it can be seen to be in close agreement with the results in [21].

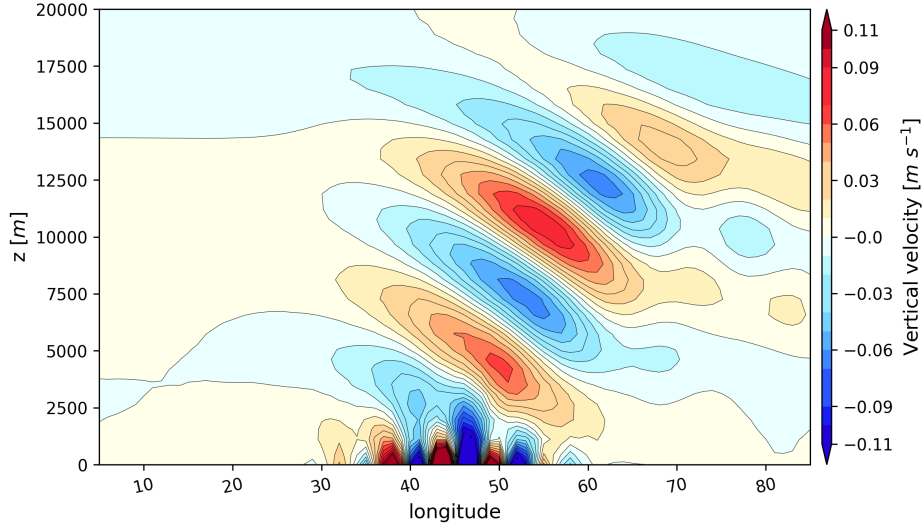


Figure 2: Vertical velocity along equator after 120 minutes simulation of the mountain ridge case. The vertical velocity contour interval is  $0.01 \text{ m/s}$ .

### 3.2.2. Circular Mountain Case

For this case, we consider uniform flow over a circular mountain of height  $250 \text{ m}$ . Using third-order spectral element polynomials, we set our model top at  $30 \text{ km}$  with 118 vertical levels (39 elements) for approximately  $250 \text{ m}$  spacing and consider a horizontal grid spacing of  $0.55$  degree (approx.  $360 \text{ m}$ ) using 56 elements per face of the cubed sphere which puts us in the nonhydrostatic regime. Figure 3 shows the modeled vertical velocity along the equator after 120 min integration using the exponential Euler method with a  $30 \text{ s}$  time step.

It is clear that the exponential integrator is able to capture the gravity waves consisting of both the larger-scale hydrostatic waves (propagating vertically) and the smaller-scale nonhydrostatic waves (propagating downstream). Comparing this modeled solution (Figure 3) with the results from Fig. 4/5 of [21] indicate that the simulations with the exponential scheme(s) reproduce all the essential features of this case.

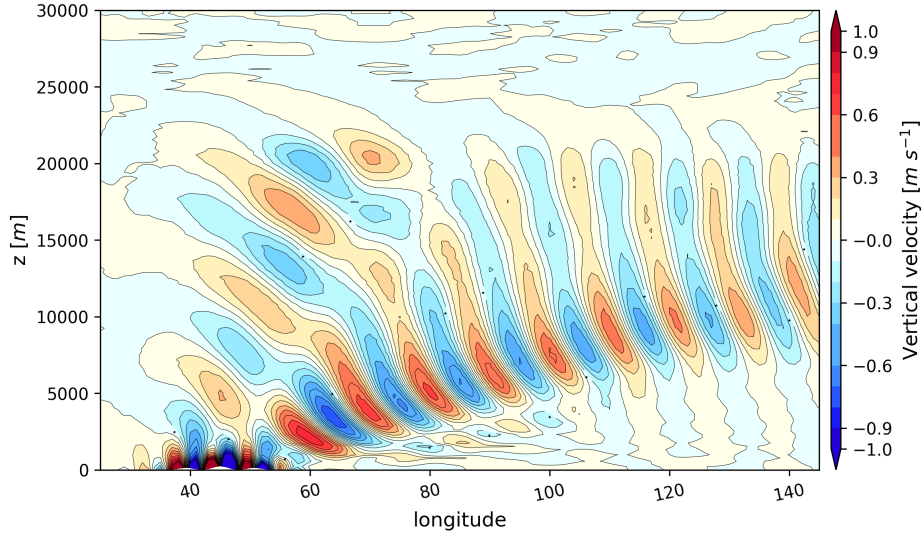


Figure 3: Vertical velocity along equator after 120 minutes simulation of the circular mountain case. The vertical velocity contour interval is 0.1  $m/s$ .

### 3.3. Baroclinic Instability

A commonly used idealized test for model developers is baroclinic instability [44]. The test consists of making a very small amplitude perturbation on an unstable zonal jet to an initially balanced state such that it triggers the development (over several days) of a baroclinic wave in the northern hemisphere. The instability appears near day five and reaches maturity day nine in the simulation and continues to grow over a 15-day simulation. Here, we will employ *EXP2* and assess how it responds to a controlled baroclinic instability.

Our numerical setup for this test case uses third-order spectral element polynomials, 32 elements per edge of the cubed sphere, and 31 vertical elements with a model top of 30  $km$ . This discretization corresponds to  $1^\circ$  (approx. 111  $km$ ) horizontal grid spacing and near 1.03  $km$  in the vertical. The exponential Euler method was used to propagate the solution in time using a time step of 360  $s$ . Figure 4 displays the surface pressure and the 850 hPa relative vorticity at days 8 and 10 of the simulation from which the baroclinic instability can be seen to be well underway and in agreement with the results in [44]. A plot of the minimum surface pressure over the 15-day simulation is provided in Figure 5; showing the evolution of the minimum surface pressure is within the packet of solutions from the suite of dynamical cores tested in [44].

### 3.4. Real-Data Forecast

We conclude our numerical experiments with a real-data simulation that confirms exponential integrators are suitable for NWP applications. The simulations presented here specified a model top of 51  $km$  (with an upper boundary absorbing layer of depth 10  $km$ ) using 32 elements per face of the cubed sphere, 3rd order polynomials, and 64 vertical levels (21 elements) which corresponds to  $1^\circ$  (111  $km$ ) horizontal grid spacing and approximately 0.8  $km$  in the vertical. Using initial conditions that were interpolated to the NEPTUNE grid from NOAA Environmental Modeling System (NEMS) / (FV3-GFS) data on 0000 UTC 1 January 2019, we ran a 96-hour forecast using *EXP2* with a 30 second time step using the GFS physics [39]. To show that we obtain a reasonable forecast, we ran a second simulation using the horizontally-explicit-vertically-implicit (HEVI) implementation [9] of the 2nd-order additive Runge-Kutta method *ars232* [1]. It is important to note that the time step size was chosen to be compatible with the physics as tuned for the *ars232*, and larger time steps can be accommodated by sub-stepping the physics (see conclusion).

Figure 6 displays the wind speed and geometric heights at 24 hour increments of the forecast for *EXP2* and *ars232*. It is clear that *EXP2* captures the large-scale flow of the mid-latitude jets, and upon comparison with *ars232*, we see the same large-scale features, including a large-scale omega block in the North Atlantic (for further discussion of the synoptic setup see [47]). Thus, exponential methods are able to run with full physics and produce realistic forecasts.

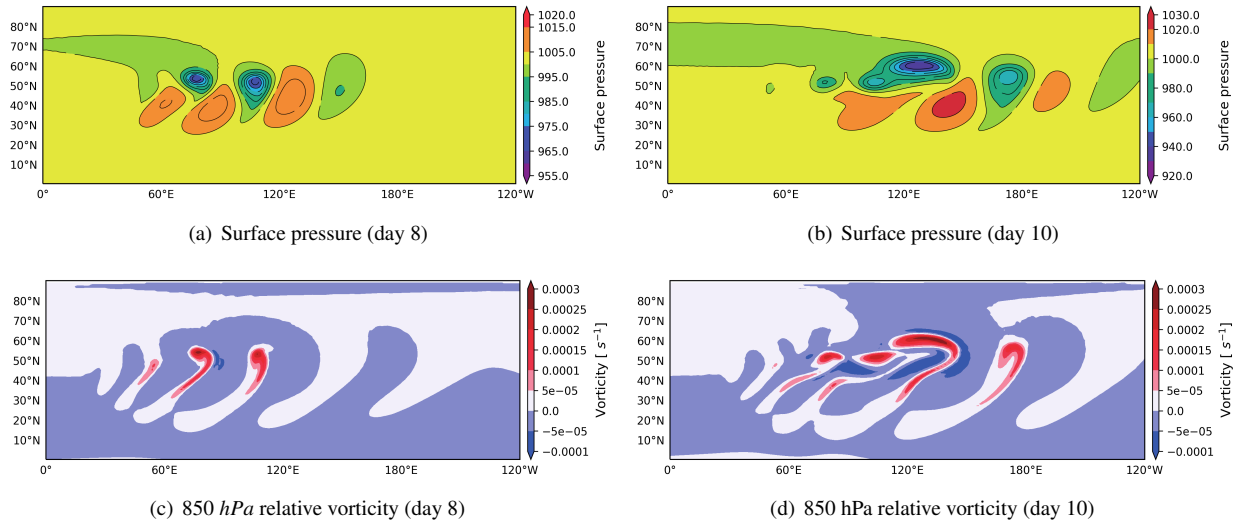


Figure 4: Surface pressure (top row) and 850 hPa relative vorticity (bottom row) shown at days 8 (left column) and 10 (right column) of the baroclinic instability simulation.

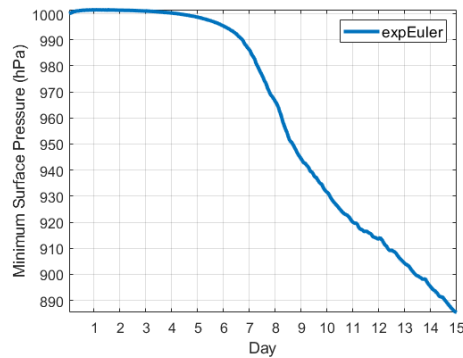


Figure 5: Time-series plot of the minimum surface pressure over the 15 day baroclinic instability simulation

#### 4. Summary and conclusions

Using the Navy's next generation numerical weather prediction system, NEPTUNE, we demonstrated that exponential methods are suitable time integrators for 3D compressible deep-atmosphere nonhydrostatic models. Taking advantage of the stability of exponential integrators, we showed that large time steps can be taken while still resolving both the large- and small- scale dynamics. The idealized test case simulations are comparable to those in the literature and provide the necessary confirmation that exponential methods are able to accurately simulate both hydrostatic and nonhydrostatic processes. Additionally, the real data experiment indicates the ability to handle the coupling of physics with dynamics and produce forecasts that align closely with the *ars232* IMEX time integrator at the same time step size.

It is of future work to conduct comprehensive comparisons with other time integrators and sub-stepping of the physics. Preliminary results suggest that *EXP2* can be competitive with IMEX and split-explicit time integration schemes. We do note that the methods of order four presented here are deemed too costly due to the fact that they require two Krylov projections per time step. However, [10] recently developed exponential multistep methods up to order six that require only a single Krylov projection per time-step. These methods are of great interest as the high accuracy complements the spectral element spatial discretization with a computational cost comparable to *EXP2*.



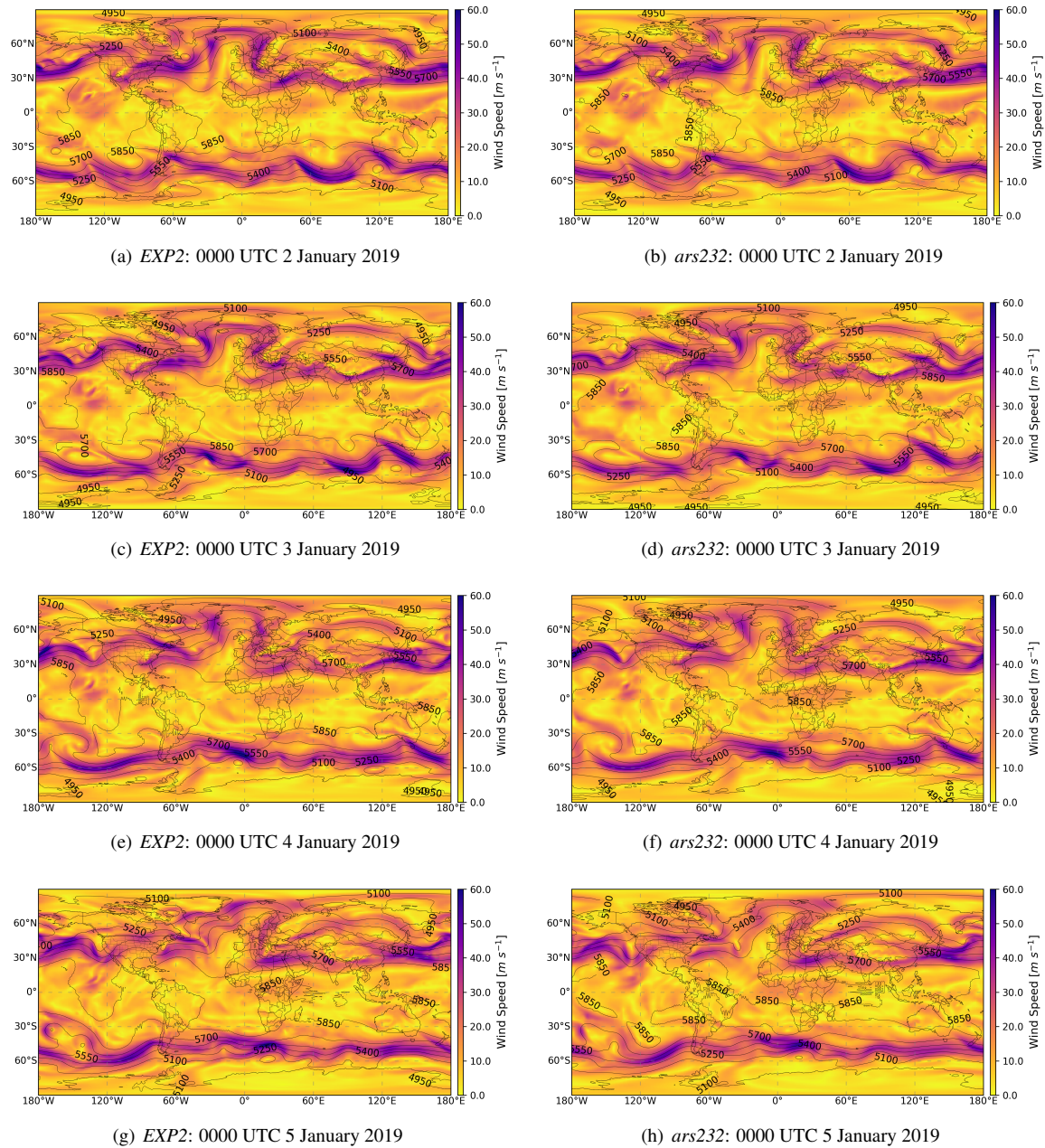


Figure 6: Real data simulation initialized on 0000 UTC 1 January 2019. The shading denotes the wind speed and contours represent the geometric height at 500 hPa with a contour interval of 150 m

## Acknowledgments

This work was supported by an American Society for Engineering Education Postdoctoral Fellowship and the Office of Naval Research 6.1-IDPI (Program Element 0601153N).

## Appendix A. Analysis of the absorbing upper boundary layer for exponential methods

Our analysis is based on partitioning

$$\frac{\partial \mathbf{u}}{\partial t} = f(t, \mathbf{u}(t)), \quad \mathbf{u}(t_0) = \mathbf{u}_0, \quad \mathbf{u}(t) \in \mathbb{R}^n \quad (\text{A.1})$$

as

$$\frac{\partial \mathbf{u}}{\partial t} = \underbrace{\{f(t, \mathbf{u}) - L\mathbf{u}\}}_{N(t, \mathbf{u})} + [L\mathbf{u}] \quad (\text{A.2})$$

where  $L$  is a linear operator that contains the terms responsible for the fast acoustic and gravity waves. The exponential Euler scheme for the partitioned problem (A.2) is given by

$$\mathbf{u}(t_n + h_n) \approx \mathbf{u}(t_n) + \varphi_1(h_n L) h_n (L\mathbf{u}(t_n) + N(t_n, \mathbf{u}(t_n))). \quad (\text{A.3})$$

For ease in presenting our analysis, we re-rewrite the adjustment (9) as a pre-time step adjustment:

$$\begin{cases} \widehat{\mathbf{u}}^n = \mathbf{Q}\mathbf{u}^n \\ \mathbf{u}^{n+1} = \widehat{\mathbf{u}}^n + h_n \varphi_1(h_n L) (N(t_n, \widehat{\mathbf{u}}^n) + L\widehat{\mathbf{u}}^n) \end{cases}, \quad (\text{A.4})$$

where  $\mathbf{Q} = \text{diag}[1, 1, 1, (1 + h_n R_w)^{-1}, 1]$ .

We note that method (A.3) is first-order accurate. Our analysis is based on the linear *IMEX* formulation [13] which considers a splitting of the density  $\rho(\mathbf{x}, t) = \rho_0(\mathbf{x}) + \rho'(\mathbf{x}, t)$ , potential temperature  $\theta(\mathbf{x}, t) = \theta_0(\mathbf{x}) + \theta'(\mathbf{x}, t)$ , and pressure  $P(\mathbf{x}, t) = P_0(\mathbf{x}) + P'(\mathbf{x}, t)$ , where the reference values are in hydrostatic balance. We then consider the partitioning (A.2) with the linear operator defined as

$$L(\mathbf{u}) = - \begin{pmatrix} w \frac{d\rho_0}{dr} + \rho_0 \frac{\partial w}{\partial r} \\ 0 \\ 0 \\ \frac{1}{\rho_0} \frac{\partial P'}{\partial r} + g \frac{\rho'}{\rho_0} \\ w \frac{d\theta_0}{dr} \end{pmatrix}, \quad (\text{A.5})$$

where  $w$  is the vertical velocity,  $r$  is the radial direction from the center of the sphere,  $g$  is gravity, and the pressure is defined via the linearization of the equation of state

$$P = p_{ref} \left( \frac{\rho R \theta}{p_{ref}} \right)^\gamma, \quad (\text{A.6})$$

as

$$P' = G_0 \rho' + H_0 \theta' \quad (\text{A.7})$$

with

$$G_0 = \frac{\gamma P_0}{\rho_0} \quad (\text{A.8})$$

$$H_0 = \frac{\gamma P_0}{\theta_0}, \quad (\text{A.9})$$

and where  $R = c_p - c_v$  is the specific gas constant,  $c_p$  and  $c_v$  are mass specific heats at constant pressure and volume, and  $\gamma = c_p/c_v$ .

We begin with the derivation of the dominant damping terms for the first order exponential scheme (A.3) and then show that we obtain the same terms for any higher-order exponential Runge-Kutta scheme. At time  $t_n$ , we make an

adjustment to our solution  $\mathbf{u}^n$ :

$$\widehat{\mathbf{u}}^n = \mathbf{Q}\mathbf{u}^n = \begin{pmatrix} \rho^n \\ w^n \\ v^n \\ (1 + h_n R_w)^{-1} w^n \\ \theta^n \end{pmatrix}. \quad (\text{A.10})$$

Using the approximation  $(1 + z)^{-1} \approx 1 - z$ , our adjustment (A.10) can be expressed as

$$\widehat{\mathbf{u}}^n = \mathbf{u}^n - h_n \begin{pmatrix} 0 \\ 0 \\ 0 \\ R_w w^n \\ 0 \end{pmatrix}. \quad (\text{A.11})$$

Inserting (A.11) into (A.4) for  $\mathbf{u}^n$  we obtain (via linearity of  $L$  and some re-arranging)

$$\mathbf{u}^{n+1} = \mathbf{u}^n + h_n \varphi_1(h_n L) (L\mathbf{u}^n + N(t_n, \widehat{\mathbf{u}}^n)) - \underbrace{h_n \begin{pmatrix} 0 \\ 0 \\ 0 \\ R_w w^n \\ 0 \end{pmatrix} - h_n^2 \varphi_1(h_n L) \begin{pmatrix} 0 \\ 0 \\ 0 \\ R_w w^n \\ 0 \end{pmatrix}}_{\text{damping terms}}. \quad (\text{A.12})$$

The last two terms on the right of (A.12) are responsible for the absorption of gravity waves and are, therefore, our primary focus. The first of these terms produces the Raleigh damping term in the vertical momentum equation. Using the Taylor series expansion of

$$\varphi_1(z) = \frac{e^z - 1}{z} = 1 + \frac{z}{2!} + \frac{z^2}{3!} + \frac{z^3}{4!} + \dots$$

we can express the last term on the right-hand-side of (A.12) as

$$h_n^2 \varphi_1(h_n L) \begin{pmatrix} 0 \\ 0 \\ 0 \\ R_w w^n \\ 0 \end{pmatrix} = h_n^2 L \begin{pmatrix} 0 \\ 0 \\ 0 \\ R_w w^n \\ 0 \end{pmatrix} + \frac{h_n^3}{2!} L^2 \begin{pmatrix} 0 \\ 0 \\ 0 \\ R_w w^n \\ 0 \end{pmatrix} + \dots, \quad (\text{A.13})$$

for which the following damping terms are obtained

$\rho'$ :

$$-h_n^2 \left( \frac{d\rho_0}{dr} R_w w^n + \rho_0 \frac{\partial}{\partial r} (R_w w^n) \right) + \mathcal{O}(h_n^3) \quad (\text{A.14})$$

$w$ :

$$h_n^3 \left[ \left( \frac{1}{\rho_0} \frac{d}{dr} \left( G_0 \frac{d\rho}{dr} + H_0 \frac{d\theta_0}{dr} \right) + \frac{g}{\rho_0} \frac{d\rho_0}{dr} \right) R_w w^n + \left( \frac{1}{\rho_0} \left( G_0 \frac{\rho_0}{dr} + H_0 \frac{d\theta_0}{dr} \right) + \frac{1}{\rho_0} \frac{d}{dr} (G_0 \rho_0) + g \right) \frac{\partial}{\partial r} (R_w w^n) + G_0 \rho_0 \frac{\partial^2}{\partial r^2} (R_w w^n) \right] + \mathcal{O}(h_n^4) \quad (\text{A.15})$$

$\theta'$ :

$$-h_n^2 \frac{d\theta_0}{dr} R_w w^n + \mathcal{O}(h_n^3) \quad (\text{A.16})$$

Upon inserting (A.15) into (A.12), we can express our vertical momentum equation as

$$\begin{aligned}
\frac{\partial w}{\partial t} \approx \mathbf{P} \left( \frac{\mathbf{u}^{n+1} - \mathbf{u}^n}{h_n} \right) &= \mathbf{P} (\varphi_1(h_n L)(L\mathbf{u}^n + N(\widehat{\mathbf{u}}^n))) - R_w w^n - h_n^2 \left[ \left( \frac{1}{\rho_0} \frac{d}{dr} \left( G_0 \frac{d\rho}{dr} + H_0 \frac{d\theta_0}{dr} \right) + \frac{g}{\rho_0} \frac{d\rho_0}{dr} \right) R_w w^n \right. \\
&+ \left. \left( \frac{1}{\rho_0} \left( G_0 \frac{\rho_0}{dr} + H_0 \frac{d\theta_0}{dr} \right) + \frac{1}{\rho_0} \frac{d}{dr} (G_0 \rho_0) + g \right) \frac{\partial}{\partial r} (R_w w^n) \right. \\
&+ \left. G_0 \rho_0 \frac{\partial^2}{\partial r^2} (R_w w^n) \right] + \mathcal{O}(h_n^3), \tag{A.17}
\end{aligned}$$

where  $\mathbf{P}$  is a 5 by 5 projection matrix with  $\mathbf{P}_{44} = 1$  and  $\mathbf{P}_{ij} = 0$ . Thus the adjustment (9) to the vertical velocity produces not only the Raleigh damping term  $R_w w^n$ , but also second order terms (in time) that includes a vertical diffusion-like term  $G_0 \rho_0 \frac{\partial^2}{\partial r^2} (R_w w^n)$  (cf. [19]). The same damping terms are obtained for higher-order Runge-Kutta methods as they can be viewed as a perturbation of the exponential Euler scheme (A.3).

## References

- [1] Uri M. Ascher, Steven J. Ruuth, and Raymond J. Spiteri, *Implicit-explicit runge-kutta methods for time-dependent partial differential equations*, Applied Numerical Mathematics **25** (1997), no. 2, 151–167, Special Issue on Time Integration.
- [2] Colm Clancy and Janusz A. Pudykiewicz, *A class of semi-implicit predictor–corrector schemes for the time integration of atmospheric models*, Journal of Computational Physics **250** (2013), 665 – 684.
- [3] S.M. Cox and P.C. Matthews, *Exponential time differencing for stiff systems*, J. Comput. Phys. **176** (2002), 430–455.
- [4] H. A. Van der Vorst, *An iterative solution method for solving  $f(A) = b$  using Krylov subspace information obtained for the symmetric positive definite matrix  $A$* , J. Comput. Appl. Math. **18** (1987), 249–263.
- [5] Lukas Einkemmer, Mayya Tokman, and John Loffeld, *On the performance of exponential integrators for problems in magnetohydrodynamics*, Journal of Computational Physics **330** (2017), 550 – 565.
- [6] R. A. Friesner, L. S. Tuckerman, B. C. Dornblaser, and T. V. Russo, *A method for exponential propagation of large systems of stiff nonlinear differential equations*, J. Sci. Comput. **4** (1989), 327–354.
- [7] J.M. Keiser G. Beylkin and L. Vozovoi, *A new class of time discretization schemes for the solution of nonlinear PDEs*, J. Comput. Phys. **147** (1998), 362–387.
- [8] E. Gallopoulos and Y. Saad, *Efficient solution of parabolic equations by Krylov approximation methods*, SIAM J. Sci. Stat. Comp **13** (1992), 1236–126429.
- [9] D. J. Gardner, J. E. Guerra, F. P. Hamon, D. R. Reynolds, P. A. Ullrich, and C. S. Woodward, *Implicit-explicit (IMEX) Runge-Kutta methods for non-hydrostatic atmospheric models*, Geosci. Model Dev. **11** (2018), 1497–1515.
- [10] Stéphane Gaudreault, Martin Charron, , Valentin Dallerit, and Mayya Tokman, *High-order numerical solutions to the shallow-water equations on the rotated cubed-sphere grid*, Journal of Computational Physics (2021).
- [11] Stéphane Gaudreault and Janusz A. Pudykiewicz, *An efficient exponential time integration method for the numerical solution of the shallow water equations on the sphere*, Journal of Computational Physics **322** (2016), 827 – 848.
- [12] Stéphane Gaudreault, Greg Rainwater, and Mayya Tokman, *Kiops: A fast adaptive krylov subspace solver for exponential integrators*, Journal of Computational Physics **372** (2018), 236 – 255.

- [13] F. X. Giraldo, J. F. Kelly, and E. M. Constantinescu, *Implicit-explicit formulations of a three-dimensional non-hydrostatic unified model of the atmosphere (NUMA)*, SIAM J. Sci. Comput. **35** (2013), B1162–B1194.
- [14] F. X. Giraldo, M. Restelli, and M. Laeuter, *Semi-implicit formulations of the Navier-Stokes equations: application to nonhydrostatic atmospheric modeling*, SIAM J. Sci. Comput. **32** (2010), 3394–3425.
- [15] M. Hochbruck, Ch. Lubich, and H. Selhofer, *Exponential integrators for large systems of differential equations*, SIAM J. Sci. Comput. **19** (1998), 1552–1574.
- [16] M. Hochbruck and A. Ostermann, *Exponential integrators of Rosenbrock-type*, Oberwolfach Reports **3** (2006), 1107–1110.
- [17] ———, *Exponential multistep methods of Adams-type*, Bit Numer Math **51** (2011), 889–908.
- [18] A.K. Kassam and L.N. Trefethen, *Fourth-order time stepping for stiff PDEs.*, SIAM J. Sci. Comput. **26** (2005), no. 4, 1214–1233.
- [19] J. B. Klemp, J. Dudhia, and A. D. Hassiotis, *An upper gravity-wave absorbing layer for nwp applications*, Monthly Weather Review **136** (2008), no. 10, 3987–4004.
- [20] J. B. Klemp, W. C. Skamarock, and J. Dudhia, *Conservative split-explicit time integration methods for the compressible nonhydrostatic equations*, Monthly Weather Review **135** (2007), no. 8, 2897–2913.
- [21] J. B. Klemp, W. C. Skamarock, and S.-H. Park, *Idealized global nonhydrostatic atmospheric test cases on a reduced-radius sphere*, Journal of Advances in Modeling Earth Systems **7** (2015), no. 3, 1155–1177.
- [22] Klemp, J. B., R. B. Wilhelmson, *The simulation of three-dimensional convective storm dynamics*, J. Atmos. Sci. **35** (1978), 1070–1096.
- [23] S. Krogstad, *Generalized integrating factor methods for stiff PDEs*, J. Comp. Phys. **203** (2005), 72–88.
- [24] M. Kwizak and A. Robert, *A semi-implicit scheme for grid point atmospheric models of the primitive equations*, Monthly Weather Review **99** (1971), no. 1, 32–36.
- [25] Vu Thai Luan, *Fourth-order two-stage explicit exponential integrators for time-dependent pdes*, Applied Numerical Mathematics **112** (2017), 91 – 103.
- [26] Vu Thai Luan and Alexander Ostermann, *Exponential rosenbrock methods of order five — construction, analysis and numerical comparisons*, Journal of Computational and Applied Mathematics **255** (2014), 417 – 431.
- [27] Vu Thai Luan, Janusz A. Pudykiewicz, and Daniel R. Reynolds, *Further development of efficient and accurate time integration schemes for meteorological models*, Journal of Computational Physics **376** (2019), 817 – 837.
- [28] Vu Thai Luan, Mayya Tokman, and Greg Rainwater, *Preconditioned implicit-exponential integrators (imexp) for stiff pdes*, Journal of Computational Physics **335** (2017), 846 – 864.
- [29] Dominik L. Michels, Vu Thai Luan, and Mayya Tokman, *A stiffly accurate integrator for elastodynamic problems*, ACM Trans. Graph. **36** (2017), no. 4, 116:1–116:14.
- [30] A. Nauts and R. E. Wyatt, *New approach to many-state quantum dynamics: the recursive-residue-generation method*, Phys. Rev. Lett. **51** (1983), 2238–2241.
- [31] Jitse Niesen and Will M. Wright, *Algorithm 919: A Krylov Subspace Algorithm for Evaluating the  $\exp(-tA)$  Functions Appearing in Exponential Integrators*, ACM Trans. Math. Softw. **38** (2012), no. 3, 22:1–22:19.
- [32] T. J. Park and J. C. Light, *Unitary quantum time evolution by iterative Lanczos reduction*, J. Chem. Phys. **85** (1986), 5870–5876.

- [33] G. Rainwater and M. Tokman, *A new class of split exponential propagation iterative methods of Runge-Kutta type (sEPIRK) for semilinear systems of ODEs*, Journal of Computational Physics **269** (2014), 40–60.
- [34] ———, *A new approach to constructing efficient stiffly accurate EPIRK methods*, Journal of Computational Physics **323** (2016), 283–309.
- [35] Greg Rainwater and Mayya Tokman, *Designing efficient exponential integrators with epiRK framework*, AIP Conference Proceedings **1863** (2017), no. 1, 020007.
- [36] André Robert, *The integration of a spectral model of the atmosphere by the implicit method*, Proc. WMO–IUGG Symp. on Numerical Weather Prediction **VII** (1969), 19–24.
- [37] Steven J. Ruuth, *Global optimization of explicit strong-stability-preserving runge-kutta methods*, Mathematics of Computation **75** (2006), no. 253, 183–207.
- [38] Christoph Schär, Daniel Leuenberger, Oliver Fuhrer, Daniel Lüthi, and Claude Girard, *A new terrain-following vertical coordinate formulation for atmospheric prediction models*, Monthly Weather Review **130** (2002), no. 10, 2459–2480.
- [39] J. Schramm, L. Bernardet, L. Carson, G. Firl, D. Heinzeller, L. Pan, , and M. Zhang, *CCPP technical documentation*, Tech. report, NCAR, 2020.
- [40] Skamarock, W. C., J. B. Klemp,, *The stability of timesplit numerical methods for the hydrostatic and the nonhydrostatic elastic equations*, Monthly Weather Review **120** (1992), 2109–2127.
- [41] M. Tokman, *Efficient integration of large stiff systems of ODEs with exponential propagation iterative (EPI) methods*, Journal of Computational Physics **213** (2006), 748–776.
- [42] ———, *A new class of exponential propagation iterative methods of Runge-Kutta type (EPIRK)*, Journal of Computational Physics **230** (2011), no. 24, 8762–8778.
- [43] Paul Ullrich and Christiane Jablonowski, *Operator-split runge–kutta–rosenbrock methods for nonhydrostatic atmospheric models*, Monthly Weather Review **140** (2012), no. 4, 1257–1284.
- [44] Paul A. Ullrich, Thomas Melvin, Christiane Jablonowski, and Andrew Staniforth, *A proposed baroclinic wave test case for deep- and shallow-atmosphere dynamical cores*, Quarterly Journal of the Royal Meteorological Society **140** (2014), no. 682, 1590–1602.
- [45] Paul Aaron Ullrich, Christiane Jablonowski, James Kent, Peter Hjort Lauritzen, Ramachandran D Nair, and Mark A Taylor, *Dynamical Core Model Intercomparison Project (DCMIP) 2012 Test Case Document*, v.1.7., Tech. report, UCAR, 2012.
- [46] Louis J. Wicker and William C. Skamarock, *Time-splitting methods for elastic models using forward time schemes*, Monthly Weather Review **130** (2002), no. 8, 2088–2097.
- [47] Kamilya Yessimbet, Albert Ossó, Rainer Kaltenberger, Linus Magnusson, and Andrea K. Steiner, *Heavy alpine snowfall in january 2019 connected to atmospheric blocking*, Weather **n/a**, no. n/a.